DOI 10.1007/s11182-018-1564-6

Russian Physics Journal, Vol. 61, No. 8, December, 2018 (Russian Original No. 8, August, 2018)

ALUMINUM ION BEAM TREATMENT OF ZIRCONIUM CERAMICS

S. A. Gyngazov, A. I. Ryabchikov, V. Kostenko, and D. O. Sivin UDC 633.3

The paper presents the radiation and thermal treatment of zirconium ceramics with high-energy Al *ion beams generated at an accelerating voltage of 1.5 kV, which modifies the structure and electrophysical properties of zirconium ceramics. Compact powder and ceramic samples are used for the radiation and thermal treatment performed at 1123–1173 K. The surface treatment of compact powders leads to the increase in the grain size, whereas the surface of ceramic samples turns black and electrically conductive in depth. This is because the change in the oxygen stoichiometry of zirconium ceramics. Air annealing of treated ceramics returns the sample to the initial state. The phase composition, microhardness and density of ceramic samples display no changes after the radiation and thermal treatment. Under the experimental conditions, the diffusion of aluminum ions in the surface layer is not observed. It is found that the ion beam treatment leads to the decrease in aluminum-containing impurity in the surface layers of zirconium ceramics.*

Keywords: zirconium ceramics, ion beam, aluminum, radiation and thermal treatment.

INTRODUCTION

The ion beam treatment is widely used for the surface modification of metals and alloys [1–4]. For several years great effort has been devoted to the study of structure and properties modifications of ceramic materials exposed to the ion beam treatment [5–9]. Still, there are no a clear idea of mechanisms of the surface modification of non-metallic materials. The accelerated ion energy and the power density in the incident ion-beam direction can vary in a wide range and are determined by technical capacities of accelerators. In this connection, it is rather relevant to address a problem of selecting optimum conditions of the ion beam treatment which will ensure its high efficiency for ceramic materials. The penetration depth of accelerated ions depends on their energy and the material density. Usually, the ion projected range does not exceed the depth of a few microns. Numerical estimates based on various methods [10, 11] prove this fact. At the same time, previous research [12–16] demonstrates that the depth of the modified layer in metals and alloys exceeds the ion penetration depth. This fact suggests the effect of long-range interaction characteristic to the ion beam-assisted modification.

The ion bombardment of materials is performed in vacuum. Up-to-date ion accelerators can generate power pulse ion beams, thereby providing power density on the order of kW/cm^2 and higher [17–19] at which the surface erosion and fusion are observed. Power pulse ion beams are mainly used to modify the properties of metals and alloys [20–25]. In several publications [6, 7, 9] it is shown that the ion beam-assisted surface modifications occur in ceramic materials. In addition to the surface erosion and fusion, the crack formation appears in ceramic materials. This can be explained by their low thermal conductivity. The ion beam treatment causes the local overheating which provides the formation of large temperature gradients and, consequently, crack formation throughout the depth of the overheated surface layer. The pulsed ion beam treatment is rather a contributory factor to the crack propagation which creates the

National Research Tomsk Polytechnic University, Tomsk, Russia, e-mail: ghyngazov@tpu.ru; ralex@tpu.ru; kostenkova@tpu.ru; sivin@tpu.ru. Translated from Izvestiya Vysshikh Uchebnykh Zavedenii, Fizika, No. 8, pp. 131–137, August, 2018. Original article submitted May 31, 2018.

largest temperature gradients. Also of interest is studying the modification of properties of ceramic materials under a continuous mode of the ion beam treatment. Such a treatment should lower the probability of cracking and increase the modification effect. These investigations can provide important information on the interpretation of mechanisms of the surface modification induced by the power pulse ion beams. In our view, the ion source developed in [26] can be used for the implementation of our experiments. This ion source is capable of generating repetitively pulsed beams of various ion species the effect from which is as similar as possible to continuous ion beams.

The aim of this work is to examine the influence of thermal heating produced by repetitively pulsed, high-energy Al beams on mechanical and electrophysical properties of zirconium ceramics.

EXPERIMENTAL TECHNIQUE

Tosoh's zirconia powder $97ZrO_2 + 3Y_2O_3$ (Japan) was used to synthesize 9 mm compact powder on a PGR-10 press (Russia) *via* isostatic pressing. Ceramic samples were synthesized by sintering compact powders in a resistance furnace SNOL 12/16 (Russia) during one hour at 1673 K. The obtained ceramic samples possessed 5.85 g/cm^3 density and 2.4% porosity.

Two types of ceramic samples were exposed to the ion beam treatment: 1) type *A*, compact powder and 2) type *B*, ceramic samples synthesized from type *A* with employment of a traditional ceramic technology. The ion beam treatment was performed in a vacuum chamber of installation equipped with plasma generator and a system of high-intensity ion beam formation [26]. Plasma generator represented a vacuum arc in the axially symmetric magnetic field. In the vacuum arc discharge, 150 A current generated a continuous flow of aluminum plasma.

The approach to the formation of high-intensity ion beams was based on plasma immersion extraction and plasma acceleration of ions in the high voltage sheath with their subsequent ballistic focusing in an equipotential drift space [26]. In order to perform the plasma immersion extraction of Al ions from vacuum arc plasma, we used a net-shaped hemispherical electrode with a radius 7.5 cm. The sample was placed at 7.5 cm distance from the hemispherical electrode. The system of ion beam formation and the sample holder were connected to a high-frequency, pulsed voltage generator which generated negative bias pulses at 50 kHz frequency, 1.5 kV pulse amplitude, 10 μs pulse length, and 0.15 A/cm^2 ion beam density. Insulated thermocouple for temperature control was mounted to the opposite side of the sample. Its heating was provided by the ion beam energy and after 20 min treatment reached stationary values within 1123–1173 K. The time of the ion treatment was 60 min.

The surface morphology was observed by scanning electron microscopy (SEM) performed on a Hitachi TM-3000 instrument. The density of ceramic samples was determined by hydrostatic weighing in distilled water on Shimadzu AUW-220 D analytical balance. The microhardness testing was performed on a Zwick Roell ZHV1-M Vickers hardness tester (Germany) using Vickers pyramid diamond indentation, at a 3 N indentation load. A double-probe spreading resistance profiling [27] was used to analyze static conductivity of ceramic samples. The X-ray diffraction (XRD) analysis was carried out on the Thermo Scientific ARL X'TRA powder diffractometer. The secondary ions were measured with a PHI 6300 mass spectrometer (Physical Electronics, USA) to determine the elemental composition of ion-implanted layers.

EXPERIMENTAL RESULTS

The ion beam treatment of the type *A* samples. The treatment of ultrafine zirconia powder with Al ions leads to its compaction which indicates to the particle interaction during ceramic sintering. Under the ion beam the sample partially fractures and cracks. This process is caused by significantly high temperature gradients. As presented in Fig. 1, the grain size increases on the treated surface. On the opposite side subjected to thermal heating, the grain size does not differ from the initial.

The ion beam treatment of the type *B* samples. Before treatment, the ceramic sample possesses a white colour intrinsic to zirconium ceramics (Fig. 2*a*). After treatment, not only the surface turns black, but the whole sample

TABLE 1. Surface Morphology and Hardness Before and After Ion Implantation.

Parameters	Before treatment	After treatment	After 1273 K annealing, t = 1 h
Coherent-scattering region, nm	138	127	111
Lattice microdistortion	$1.1 \cdot 10^{-3}$	$1.2 \cdot 10^{-3}$	$1.1 \cdot 10^{-3}$
Microhardness, GPa	14.17±28	14.99±0.41	14.81±0.34

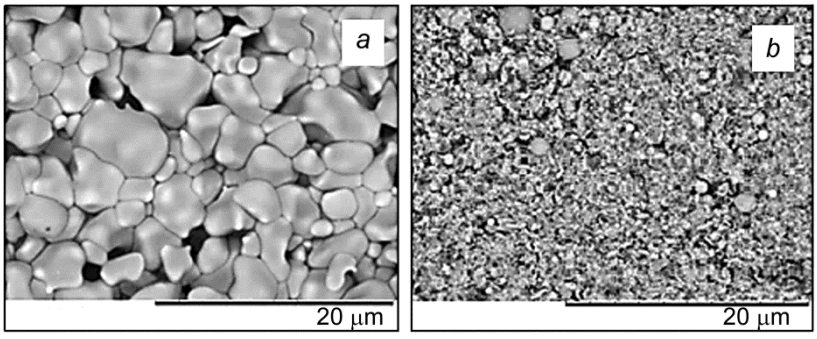

Fig. 1. Surface modification on different sides of ceramic sample: *a* – exposed to ion beam treatment, *b* – opposite side.

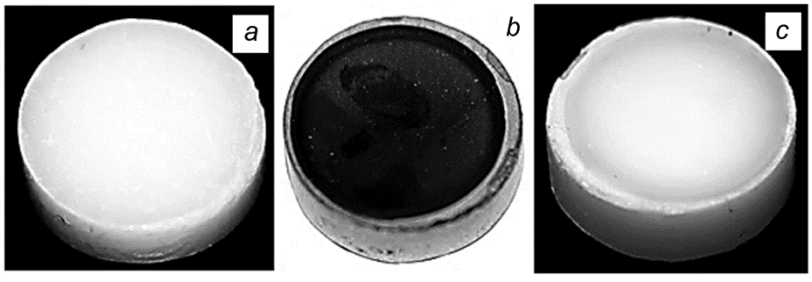

Fig. 2. Appearance of ceramic sample: *a* – before ion beam treatment; *b* – after ion beam treatment; *c* – after 1273 K air annealing during 1 h.

darkens uniformly in the depth (Fig. 2*b*). After air annealing at 1273 K during one hour, the sample again acquires white colour in the whole depth (Fig. 2*c*).

After the ion implantation, the surface layers are removed to a depth of about 150–200 μm, whereas the density and porosity of ceramic samples remain as before.

SEM observations show that the microstructure of ceramic samples does not change during the ion implantation. According to measuring results summarized in Table 1, the microhardness increases insignificantly. Thus, the microhardness before and after the ion implantation ranges within 14.17 ± 28 and 14.99 ± 0.41 GPa, respectively. After 1273 K annealing for an hour, the microhardness of ion-treated samples remains almost the same (14.81 ± 0.34 GPa).

Electrical conductivity of ceramic samples is measured before and after the ion implantation and after the intermediate annealing at 673 K during 20 min. In terms of 1 nA sensitivity of our measurement unit, ceramic samples in the initial state are non-conductive, *i.e.* measurement probes do not detect any current. After the ion beam treatment, the conductivity is detected confidently, and the first measurement gives the temperature curve *1* presented in Fig. 3. The numerical value of conductivity obtained at 323 K, is $1.17 \cdot 10^{-8}$ $(\text{Ohm} \cdot \text{cm})^{-1}$, while at 573 K it is $7.43 \cdot 10^{-6}$ $(\text{Ohm} \cdot \text{cm})^{-1}$ (Fig. 3, curve *1*). Another heating is accompanied by a slight decrease in conductivity (Fig. 3,

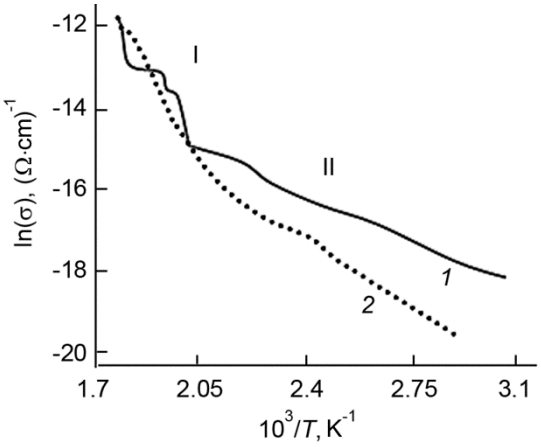

Fig. 3. Temperature curves of conductivity after ion beam treatment: *1* – first measurement, *2* – second measurement.

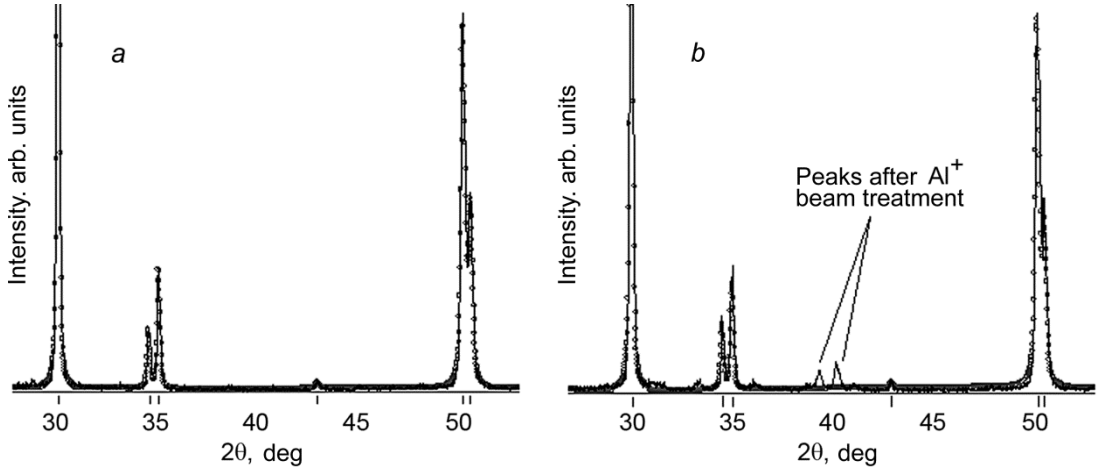

Fig. 4. XRD patterns of ceramic samples of type *B*: *a* – before ion beam treatment; *b* – after ion beam treatment.

curve *2*) which is probably determined by the oxidation process occurred during the first heating. This fact is proved by the absence of conductivity caused by 673 K intermediate annealing for 20 min, when the current between the probes is not detected even at 573 K heating.

Let us divide each curve in Fig. 3 into segments I and II having a certain angles of inclination. Using the linear approximation, in the first conductivity detection we find that the activation energy is 9.73 and 2.93 eV, respectively for segments I and II. In the second conductivity detection, the activation energy is 13 and 5.16 eV, respectively for segments I and II. In other words, with the increasing number of measurements accompanied by 573 K heating, the activation energy increases in each curve segment, which is typical for oxidation processes.

It follows that the black colour of the ion-implanted ceramic sample and the increase in its conductivity are connected with the change in oxygen stoichiometry. Oxygen release from the sample occurs due to its thermal treatment in a vacuum. Air thermal treatment leads to the recovery of the initial stoichiometric composition of the sample, which is manifested in the recovery of its originally low conductivity in addition to the original white colour.

Figure 4 presents the XRD results of ceramic samples before and after the ion beam treatment. As can be seen from this figure, the sample has a tetragonal phase both before and after the treatment. The absence of the cubic phase

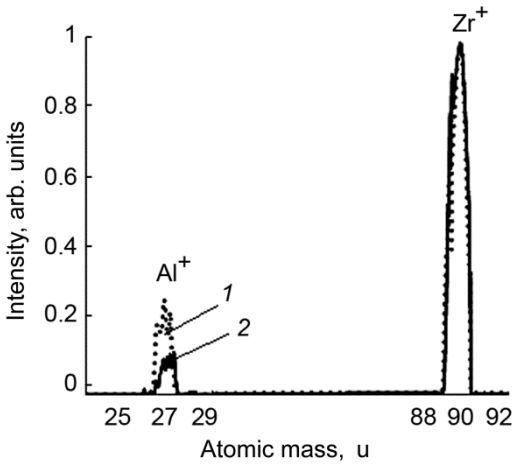

Fig. 5. Al content in surface layers of ceramic samples: *1* – before ion beam treatment; *2* – after ion beam treatment.

means that the heating of ceramic samples during the ion implantation does not exceed 2570 K [28, 29]. After the ion beam treatment, the obtained diffraction patterns are analyzed using the PowderCell 2.4 software. This analysis shows two small XRD peaks which are not typical for diffraction patterns of zirconium ceramics. These peaks disappear after annealing for one hour at 1273 K. According to the XRD analysis, the aluminum content in the surface layers of zirconium ceramics corresponds to the level of impurity.

According to Table 1, the ion implantation does not cause a significant change both in the size of the coherent-scattering region and the lattice microdistortion.

According to results of secondary ion mass spectrometry presented in Fig. 5, the amount of the Al impurity in the ion-treated surface layers is about 3.7 times less than that in the untreated layers. This value is obtained *via* the normalization of peak intensities of zirconium and aluminum before and after the ion beam treatment. The XRD peak for zirconium is taken as a unit for intensity, and the conventional content of aluminum is calculated *via* the proportion formula.

The decrease in the Al content is caused by the predominance of the ion sputtering over the diffusion of implanted ions throughout the depth of the surface layer. The melting temperature of 2323 K of aluminum oxide is considerably lower than that of zirconium dioxide (2988 K). The effective removal of aluminum oxide from the surface layer can be associated with the localized overheating up to the melting temperature induced by the ion beam treatment. Consequently, the low-melting component removes from the surface layer resulting in the reduction of the aluminum-containing impurity. Afterwards, the chemical composition of the surface layer changes. As mentioned above, the absence of the cubic phase proves the fact that the heating temperature in the surface layer does not exceed 2570 K. Therefore, the removal of the thin surface layer during the ion beam treatment occurs owing to the ion beam etching. The absence of traces of the ion diffusion in the sample depth indicates to the fact that the etching rate is substantially higher than the rate of diffusion.

CONCLUSIONS

We investigated the influence of thermal heating produced by repetitively pulsed, high-energy Al beams on mechanical and electrophysical properties of zirconium ceramics. Based on the results obtained, the following can be concluded. The treatment of ultrafine zirconia powder with Al ions was accompanied by cracking that indicated to higher temperature gradients. Also, a significant growth in the grain size was observed on the ion-implanted sample surface. The rate of the powder particle agglomeration was considerably lower on the untreated sample surface subjected only to thermal heating.

The ion beam treatment of zirconium ceramics sintered by the power pulse ion beams was not accompanied by cracking of the surface layers, which is common to the power pulse ion implantation. This kind of the ion beam treatment resulted in the sample blackening uniformly in its whole depth. This indicated to a change in the oxygen stoichiometry of zirconium ceramics, *i.e.* the reduction in the oxygen concentration due to its release into ambient air with reduced pressure of residual gases (vacuum) induced by the high temperature and the ion beam treatment. After air annealing, the ceramic sample became white again in the whole depth. This was because the recovery of the inital stoichiometric composition typical for zirconium ceramics sintered in air conditions.

The ion bean treatment did not significantly changed the porosity and microhradness of ceramic samples. Neither implantation nor diffusion of Al ions occurred in the surface layers that was proved by the XRD analysis and secondary ion mass spectrometry.

Therefore, when the radiation and thermal treatment of ceramic sample achieved 1073 K and higher, the ion sputtering predominated over the diffusion of implanted ions throughout the depth of the surface layer.

It was shown that the pulsed ion beam treatment is a promising technology of modification of ceramic surfaces and their diffusion annealing targeted at the implantation of accelerated metal ions in material to a depth substantially increasing the mean free path. In order to increase the modification effect, the conditions of the ion beam treatment should be optimized by reducing the ion sputtering over the surface layers keeping constant the concentration of metal ions in the beam. The identification of the main laws of the interaction between accelerated ions and zirconium ceramics depending on the ion beam treatment conditions requires further investigation.

This work was financially supported by Grant N 17-19-01082 from the Russian Science Foundation.

REFERENCES

1. I. Vlasov, S. Panin, V. P. Sergeev, *et al.,* Adv. Mater. Res., **872**, 219–224 (2014).
2. A. I. Ryabchikov, D. O. Sivin, P. S. Anan'in, *et al.,* Russ. Phys. J., **61**, No. 2, 270–277 (2018).
3. A. S. Demin, E. V. Morozov, S. A. Maslyaev, *et al.,* Fiz. Khim. Obrab. Mater., No. 6, 42–50 (2016).
4. I. Yu. Romanov, N. V. Gushchina, V. V. Ovchinnikov, *et al.,* Russ. Phys. J., **60**, No. 10, 1823–1831 (2018).
5. S. A. Maslyaev, E. V. Morozov, P. A. Romakhin, *et al.,* Fiz. Khim. Obrab. Mater., No. 3, 5–17 (2015).
6. I. G. Romanov and I. N. Tsareva, ZhTF, **27**, No. 16, 65–70 (2001).
7. S. A. Gyngazov, I. P. Vasil'ev, A. P. Surzhikov, *et al.,* ZhTF, **85**, No. 1, 132–137 (2015).
8. K. P. Savkin, A. S. Bugaev, A. G. Nikolaev, *et al.,* Izv. Vyssh. Uchebn. Zaved., Fiz., **57**, No. 10/3, 244–248 (2014).
9. V. Kostenko, S. Pavlov, and S. Nikolaeva, IOP Conf. Ser.: Mater. Sci. Eng., **289**, 012019 (2018).
10. A. F. Burenkov, F. F. Komarov, M. A. Kumachov, and M. M. Temkin, The Spatial Distribution of the Energy Released in a Cascade of Atomic Collisions in Solids. Energoizdat, Moscow (1985).
11. J. P. Biersack and L. G. Haggmark, Nucl. Instrum. Methods, **174**, 257–269 (1980).
12. V. V. Ovchinnikov, N. V. Gushchina, I. Yu. Romanov, *et al.,* Russ. Phys. J., **59**, No. 10, 1521–1527 (2017).
13. A. V. Markidonov, Fundamental'nye problemy radioelektronnogo priborostroeniya, **16**, No. 4. 33–36 (2016).
14. I. N. Serov, V. I. Margolin, V. A. Zhabreev, *et al.,* Inzhenernaya fizika, No. 1, 50–67 (2005).
15. S. E. Sabo, Informatsionno-tekhnologicheskii vestnik, No. 3, 119–133 (2016).
16. Yu. P. Sharkeev, N.V. Girsova, A.I. Ryabchikov, *et al*., Nucl. Inst. Methods Phys. Res. B, **106**, Nos. (1–4), 532–537 (1995).
17. A. I. Ryabchikov, P. S. Anan'in, S. V. Dektyarev, *et al.,* ZhTF, **43**, No. 23, 3–10 (2017).
18. V. A. Gribkov, A. S. Demin, E. V. Demina, *et al.,* Prikladnaya fizika, No. 3, 43–51 (2011).
19. E. A. Azizov, A. A. Airapetov, L. B. Begrambekov, *et al.,* VANT. Ser. Termoyadernyi sintez, No. 37, 30–38 (2014).
20. V. V. Uglov, G. E. Remnev, A. K. Kuleshov, and M. S. Saltymakov, Fiz. Khim. Obrab. Mater., No. 1, 65–70 (2010).
21. B. Ganavati, V. A. Kukarenko, and A. G. Kononov, Russ. Phys. J., **58**, No. 1, 63–69 (2015).
22. V. V. Ovchinnikov, F. F. Makhin'ko, and V. I. Solomonov, J. Phys.: Conf. Ser., **652**, 012070 (2015).

23. Haowen Zhong, Jie Zhang, Jie Shen, *et al.,* Nucl. Instrum. Methods Phys. Res., **409**, 298–301 (2017).
24. A. G. Konnov, V. A. Kukareko, A. V. Belyi, and Yu. P. Sharkeev, Mekhanika mashin, mekhanizmov i materialov, No. 22, 47–53 (2013).
25. V. K. Struts and G. E. Remnev, Izv. Vyssh. Uchebn. Zaved., **53**, No. 10/2, 125–128 (2010).
26. A. I. Ryabchikov, P. S. Ananin, S. V. Dektyarev, *et al.,* Vacuum, **143**, 447– 453 (2017).
27. V. P. Miroshkin, Ya. I. Panova, and V. V. Pasynkov, Phys. Solid State, **66**, 779–782 (1981).
28. V. G. Zavodinskii and A. N. Chibisov, Phys. Solid State, **48**, No. 2, 363–368 (2006).
29. A. P. Surzhikov, T. S. Frangul'yan, S. A. Gyngazov, and S. V. Grigor'ev, Izv. Vyssh. Uchebn. Zaved., Fiz., **54**, No. 1/3, 237–241 (2011).